IOP Conf. Series: Materials Science and Engineering **382** (2018) 022029 doi:10.1088/1757-899X/382/2/022029

# Establishment of hot processing map and work hardening mechanism of 0Cr11Ni$_2$MoVNb stainless steel during hot compression process

**Jia Fu[1,2], Fuguo Li[2], Yongtang LI[3]**

[1]School of Material science and engineering, Xi'an Shiyou University, Xi'an, 710065, China;

[2]School of Materials Science and Engineering, Northwestern Polytechnical University, Xi'an 710072, China;

[3]Material science and engineering, Taiyuan university of science and technology, taiyuan, 030024, China;

Email: fujia@xsyu.edu.cn

**Abstract:** True stress versus true strain curves of 0Cr11Ni$_2$MoVNb stainless steel were obtained from isothermal compression tests on Gleeble-1500 tester over a wide temperature range from 1223K to 1433K and a strain rate range from 0.01s$^{-1}$ to 10s$^{-1}$. Combined with the stress-strain data during hot deformation process, work hardening mechanism of of 0Cr11Ni$_2$MoVNb steel was investigated. Besides, the developed MATLAB code was provided to generate hot processing map to analysis the influencing rule of various deformation parameters on instability region and energy dissipation under the strain degree of 0.3, 0.5 and 0.7. The main result shows that: (1) Based on dynamic materials modeling(DMM), the processing map was established, where the flow instability maybe occur when the strain rate is higher than 0.1 s-1. (2) the temperature and strain rate range for dynamic recovery and recrystallization become lager when strain increases, besides, the globularization intensities increasing obviously with decreasing of temperature and increasing of strain rate. (3) maximum values of the deformation activation energy under various strain degree are concentrated in the deformation region with the temperature over 1373K and the strain rate nearby 0.1s-1, and then the optimum temperature and strain rate ranges for hot ring rolling at different strain of the steel are determined according to the hot processing maps.

## 1. Introduction

0Cr11Ni$_2$MoVNb is a new kind of martensitic stainless steel, which is a kind of hot rolled steel achieved by heat treatment (quenching and tempering) to adjust the performance of stainless steel, with high strength and corrosion resistance. The martensitic stainless steel can be used to make working under high temperature parts, such as steam turbine blades, gear shaft and pull rod and parts such as valve working in corrosion medium, bolts, large gas turbine engine turbine disc, etc. [1,2]. Material physical parameters can be calculated through various simulation methods to provide support for performance calculation [3-6]. The hot processing map can analyze and forecast the deformation mechanisms of materials under the various deformation parameters, such as dynamic recovery, dynamic recrystallization, superplastic deformation, crack and local flow stress. Prasad [7] has put forward a dynamic materials model (Dynamic material modeling, DMM), where the hot processing

map get the "safety zone" and "instability area" to optimize the hot processing parameters, thus to avoid certain product defects.

Until now, many scholars have studied the hot processing map of metal materials. Liu et al. [7] obtained an optimum condition for the hot working of Haynes 230 alloy. Their results showed that the alloy exhibited a good workability at the deformation temperature of 1150°C and the strain rate of $0.001s^{-1}$. Reddy et al. [9] investigated the hot working of Al–Li alloy, and pointed out two domains with peak efficiencies were associated with cracking processes due to grain boundary cavitations and flow localization. Zhang et al. [10] developed the processing maps of a P/M titanium-aluminide alloy and pointed out that superplastic deformation occurred at the deformation temperature of 1100°C and the strain rate of $0.001s^{-1}$ with peak efficiency of 60%. Wang et al.[11] found that the instability region of Ti-6.5Al-3.5Mo-1.5Zr-0.3Si alloy increased with the increasing of strain. Li and Zhang [12] investigated the hot deformation behavior of Ti-6Al-4V alloy basing on processing maps at various strains and found that hydrogen content affected the instability parameter.

At present, the research on hot processing map of metal material commonly use the traditional method to obtain the instability region by hand-painted hot processing map, ignoring the effect of work hardening rate on the processing mechanism of material. This paper will illustrate the hot processing map of $0Cr11Ni_2MoVNb$ steel by Matlab programming, and the most suitable parameters for hot processing production were obtained.

## 2. Experimental procedure and strain-stress curves

### *2.1 Experimental scheme*

The chemical compositions of $0Cr11Ni_2MoVNb$ stainless steel were (wt.%): C: 0.070, Si: 0.180, Mn: 0.380, Cr: 11.39, Ni: 1.570, Mo: 0.390, V: 0.150, Nb: 0.080, P: 0.015, S: 0.004, Fe: (balance). Cylindrical specimens with a diameter of 8 *mm* and a height of 12 *mm* were machined and with grooves of 0.2*mm* depth on both sides filled with graphite powder as lubricant to reduce friction and assure the stability and uniformity during compression testing. A computer-controlled, servo-hydraulic Gleeble 1500 machine was used for compression testing with height reduction 80% at the temperatures of 1223K, 1273K, 1323K, 1373K and 1433K, and the strain rates of 0.01 $s^{-1}$, 0.1 $s^{-1}$, 1 $s^{-1}$ and 10 $s^{-1}$. These 20 specimens were heated to 1473K at first at a heating rate of 283K/s with holding time 180s and cooled to deformation temperatures selected for the corresponding compression, and then specimens were isothermally compressed at the constant strain rates and then rapidly quenched with water to room temperature. The variations of stress and strain were recorded automatically by a personal computer equipped affixed to an automatic data acquisition system during isothermal compression. The true stress–strain curves were calculated by related formulas [13] by the nominal stress–strain curves collected.

### *2.2 Analysis of experimental stress-strain curves*

The true stress-strain curves of $0Cr11Ni_2MoVNb$ obtained by hot compression test are depicted in Figure 1.

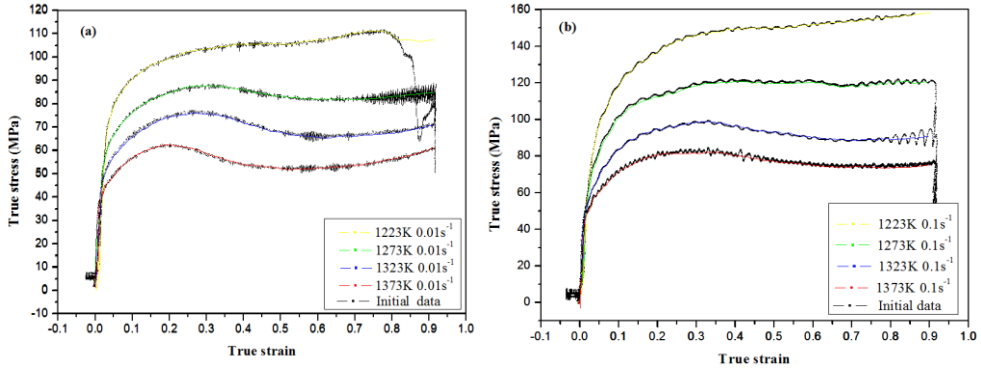

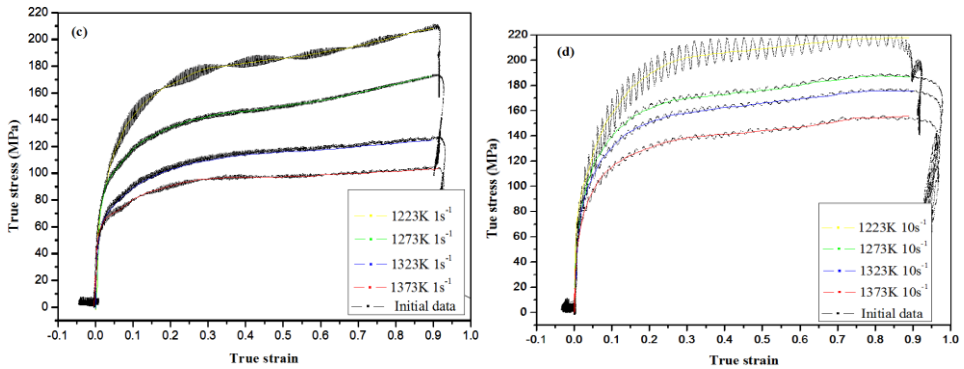


Figure 1 Flow curves of 0Cr11Ni$_2$MoVNb steel under various conditions: (a) 0.01s$^{-1}$; (b) 0.1s$^{-1}$; (c) 1s$^{-1}$; (d) 10s$^{-1}$.

As is in Figure 1, 0Cr11Ni$_2$MoVNb steel is sensitive to temperature and strain rate, and the flow stress and the shape of the flow curves is sensitively dependent on temperature and strain rate. The rheological stress curve of the 0Cr11Ni2MoVNb steel under high temperature deformation has two forms: one is the high strain rate and the low deformation temperature, and the dynamic response is presented; the other is the dynamic recrystallization with low strain rate and high deformation temperature. Test results show the typical curve of dynamic recrystallization, with the characteristics: the strain rate lower than 0.1 s$^{-1}$and temperature higher than 1273K, with the increase of strain, stress peak is reached, and then followed by softening stage.

## 3. Analysis of work hardening ratio and hot processing map

The dynamic recrystallization kinetics model is commonly established by the critical strain $\varepsilon_c$, the peak strain $\varepsilon_p$ and the steady-state strain $\varepsilon_s$. The $\varepsilon_c$ was calculated by equation: $\varepsilon_c$=0.69ε [14], and the $\varepsilon_s$ was determined by the curve of the work hardening rate θ and the strain ε [14]. For the θ-ε curve, a first-order inverse of the true stress-strain curve is obtained by the approximating method: $d\sigma/d\varepsilon \approx \Delta\sigma/\Delta\varepsilon$, thus the relationship curve between the work hardening rate and the strain under each strain rate can be obtained. The maximum flow stress of 0Cr11Ni$_2$MoVNb stainless steel is listed in Table 1.

Table 1 The maximum flow stress of 0Cr11Ni$_2$MoVNb stainless steel (unit:MPa)

| Strain rate (s-1) | Temperature (K) | | | | |
|---|---|---|---|---|---|
| | 1223K | 1273K | 1323K | 1373K | 1433K |
| 0.001 | 106.02 | 83.12 | 67.22 | 51.78 | 41.04 |
| 0.1 | 150.14 | 120.21 | 92.99 | 53.39 | 35.62 |
| 1 | 185.38 | 164.61 | 82.38 | 108.76 | 96.22 |
| 10 | 213.26 | 145.72 | 161.72 | 151.47 | 119.36 |

### *3.1 The work hardening rate under various temperatures*

The total power is described as follows [15,16]:

$$P = \sigma\dot{\varepsilon} = G + J = \int_0^{\dot{\varepsilon}} \sigma d\dot{\varepsilon} + \int_0^{\sigma} \dot{\varepsilon} d\sigma = \frac{P}{1+m} + \frac{mP}{1+m} \quad (1)$$

Where, $\dot{\varepsilon}$ is the strain rate. The dissipated power J is obtained by:

$$J = \int_0^{\dot{\varepsilon}} \sigma d\dot{\varepsilon} = \frac{m}{m+1}\sigma\dot{\varepsilon} \quad (2)$$

The value of *J* for a non-linear dissipater is normalized with that of a linear dissipater (*m*=1) to obtain an efficiency of power dissipation (EPD), given by:

$$\eta = \frac{J}{J_{\max}} = \frac{2m}{m+1} \tag{3}$$

Where, $m$ is the strain rate sensitivity exponent and can be described as follows:

$$m = \left(\frac{dJ}{dG}\right)_{T,\varepsilon} = \left(\frac{\partial \log \sigma}{\partial \log \dot{\varepsilon}}\right)_{T,\varepsilon} = \frac{\dot{\varepsilon}}{\sigma}\left(\frac{d\sigma}{d\dot{\varepsilon}}\right)_{T,\varepsilon} \tag{4}$$

The instability criterion $\xi(\dot{\varepsilon})$ is developed based on the extreme principles of irreversible thermodynamic as applied to large plastic flow [17]. This criterion represents the maximum rate of energy production, the material may generate flow instabilities when $\xi(\dot{\varepsilon}) < 0$. The instability criterion $\xi(\dot{\varepsilon})$ is as:

$$\xi(\dot{\varepsilon}) = \frac{\partial \log(m/(m+1))}{\partial \log \dot{\varepsilon}} + m < 0 \tag{5}$$

The variation of dimensionless parameters $\xi(\dot{\varepsilon})$ and $\eta$ with deformation temperature and strain rate constitutes processing map. The theoretical derivation is detailed in reference [18].

*3.2 The work hardening rate under various strain rates*

Work-hardening rate (θ)-strain (ε) curves of 0Cr11Ni$_2$MoVNb steel under various strain rates is in Figure 2.

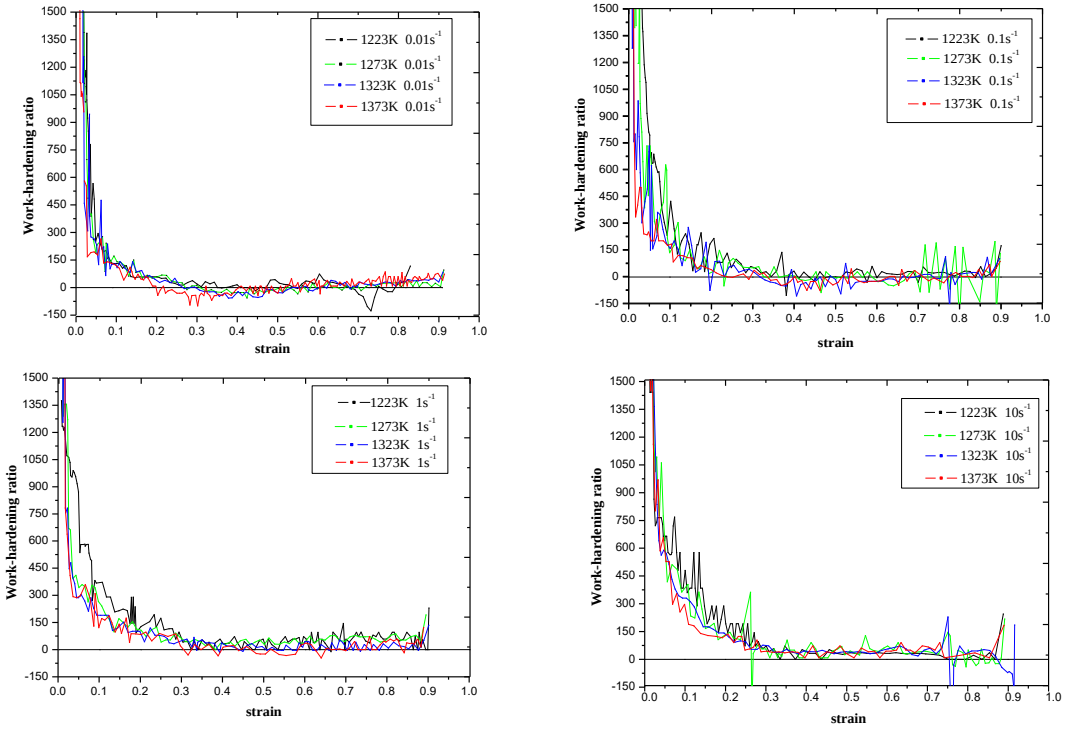


Figure 2 Work-hardening rate(θ)-strain(ε)curves of 0Cr11Ni$_2$MoVNb steel under various strain rates

As in Figure 2, with the increase of the strain, the work hardening rate reached to the maximum value then gradually reduced, then fluctuated near the zero value. The strain value where the work hardening rate in the first peak is zero was called peak strain $\varepsilon_p$. With the further increase of strain, the work hardening rate value fluctuates up and down near the zero, which is the typical cycle model of dynamic recrystallization.

When the work hardening rate is firstly restored to zero value, the corresponding strain is as the

steady-state strain $\varepsilon_s$, the two eigenvalues of $\varepsilon_p$ and $\varepsilon_s$ under different deformation conditions can be obtained. According to the relationship between the $\varepsilon_p$ and $\varepsilon_s$, the dynamic recrystallization critical strain of $\varepsilon_c$ was obtained, and the corresponding stress value by the stress - strain curve is thus read. In order to further determine the suitable hot processing parameters, the hot processing map can be drawn to determine them.

*3.3 Analysis of hot processing map*

Figure 3 shows the processing maps of 0Cr11Ni2MoVNb steel under various strains.

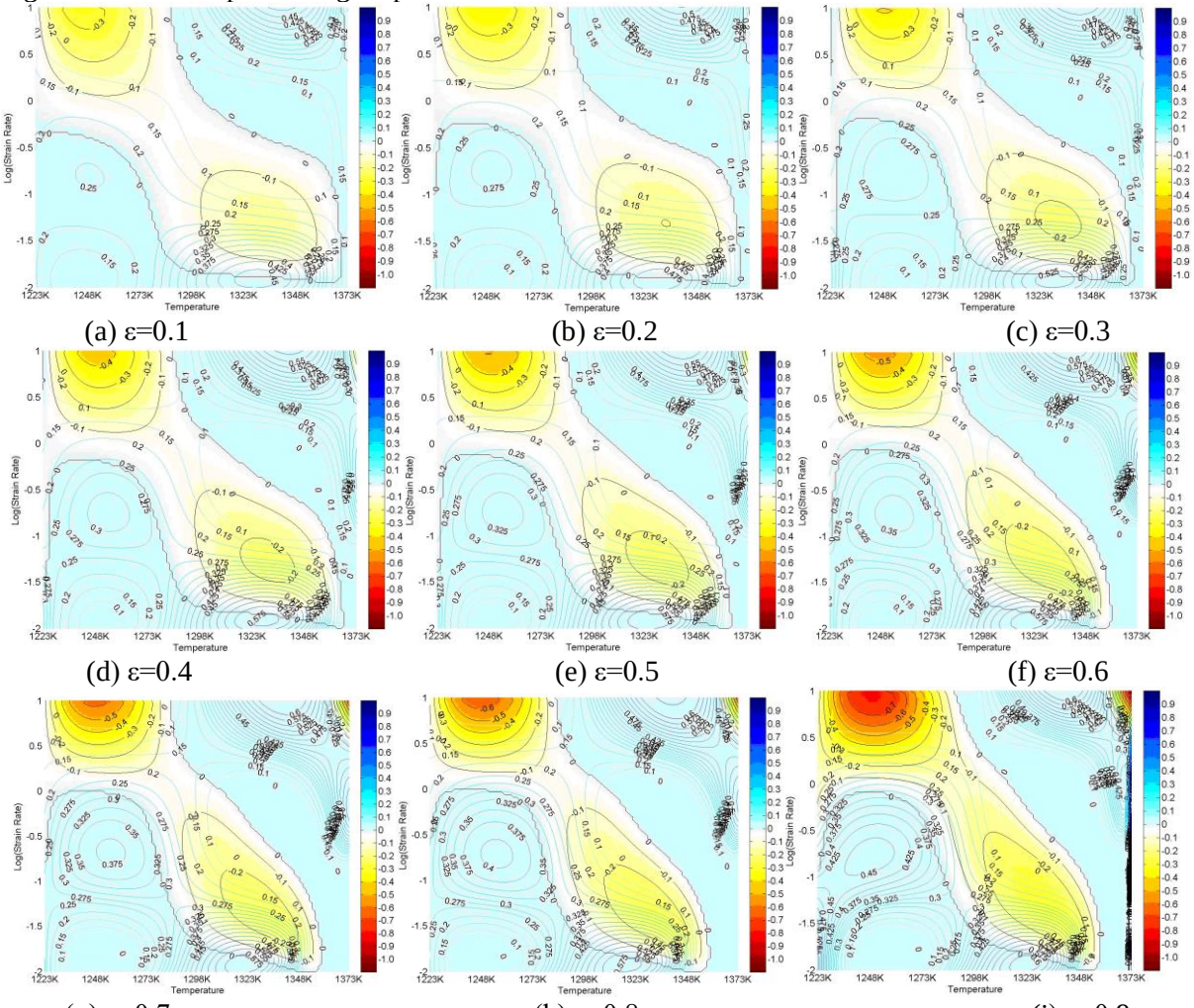


(a) ε=0.1 (b) ε=0.2 (c) ε=0.3

(d) ε=0.4 (e) ε=0.5 (f) ε=0.6

(g) ε=0.7 (h) ε=0.8 (i) ε=0.9

Figure 3 Processing maps of 0Cr11Ni2MoVNb steel under various strains

As is shown in Figure 3, the color area in the hot processing map is the rheological instability zone, and the white area is the hot working safety zone. The hot processing map depicts the process area and the hazardous area of the "safe" microstructure. And the dynamic recrystallization zone, the dynamic recovery zone and safe area are the better tissue regions for the hot deformation [19]. When the energy dissipation rate $\eta > 30\%$, the curve of energy dissipation rate changes obviously due to the dynamic recrystallization. With the decrease of the strain rate, the raised tendency of $\eta$ is basically stable within the area of lower strain rate and lower deformation temperature.

## 4. Conclusion

The isothermal compression experiment is carried out on the Gleeble-1500 machine for the specimen

of the 0Cr11Ni$_2$MoVNb martensitic stainless steel, through the data analysis and calculation, rheological behavior and hot processing map of the steel was studied and the rheological instability zone is obtained. Results are as:

(1) The characteristics of the hot processing map under low strain are similar under various strains. The instability region have appeared in the area of high deformation temperature and low strain rate, within the strain rate region of $0.05s^{-1}$~$0.1s^{-1}$ and the temperature area of 1273K~1433K. Under the experimental conditions of high strain, the instability zone appears in low deformation temperature (1223K~1273K) and high strain rate region ($1s^{-1}$~$10s^{-1}$).

(2) With the increase of deformation temperature and the decrease of strain rate, the rate of energy dissipation η is on the rise. Within the area of the low strain rate ($0.01s^{-1}$~$0.1s^{-1}$) and the deformation temperature higher than 1343K, it shows a good processing performance, within the scope of the optimized process parameters of 0Cr11Ni$_2$MoVNb steel.

(3) When the strain is less than 0.4, the instability of color area in hot processing map is in the region of higher than 1373K and lower than $0.1s^{-1}$. The instability area within the strain of 0.5~0.8 is due to the thermal unbalance under the low temperature and high strain rate, and cracks occur in the shear zone or the nearby grain boundary.

Overall, it is found that the situation of the low temperature at high strain rate and the high temperature at low strain rate are the most suitable for the hot processing production.

**Acknowledgements**

This work is supported by Natural Science Foundation of China (No.51275414, No.51174140). Thanks to the ANDA Aviation Forging Co., Ltd. for the financial support. Thanks to Qiufeng WANG for her help. Also great thank to the Aviation Industry Corporation of China (AVIC) for the experimental instruction.

**References**

[1] Lo K H, Shek C H, Lai J K L. Recent developments in stainless steels[J]. Materials Science and Engineering: R: Reports, 2009, 65(4): 39-104.

[2] Müller-B. C, Zimmermann M, Christ H J. Adjusting the very high cycle fatigue properties of a metastable austenitic stainless steel by means of the martensite content[J]. Procedia Engineering, 2010, 2(1): 1663-1672.

[3] Fu J, Fabrice B. , Siham K.B., Assessment of the elastic properties of amorphous Calcium Silicates Hydrates (I) and (II) structures by Molecular Dynamics Simulation[J]. Molecular Simulation.2017, 44(05):1-15.

[4] Fu J, Fabrice B., Siham K.B.. First-principles calculations of typical anisotropic cubic and hexagonal structures and homogenized moduli estimation based on the Y-parameter[J]. Journal of Physics and Chemistry of Solids, 2017, 101: 74-89.

[5] Fu J, Fabrice B., Siham K.B., Multiscale Modeling and Mechanical Properties of Zigzag CNT and Triple-Layer Graphene Sheet Based on Atomic Finite Element Method[J]. J. Nano Research. 2015, 33:92-105

[6] Fu J, Yongtang Li, Huiping Qi. Microstructure simulation and experimental research of as-cast 42CrMo steel during quenching process[J]. Advanced Materials Research, 2011, (317-319):19-23.

[7] PRASAD Y V R K. Hot working guide：A compendium of processing maps[M]. OH：ASM International Materials Park, 1997.

[8] Liu Y, Hu R, Li J, et al. Characterization of hot deformation behavior of Haynes230 by using processing maps[J]. Journal of Materials Processing Technology, 2009, 209(8): 4020-4026.

[9] Reddy G J, Srinivasan N et al. Processing map for hot working of spray formed and hot isostatically pressed Al–Li alloy (UL40)[J]. Journal of Materials Processing Technology, 2009, 209(18): 5964-5972.

[10] Zhang W, Liu Y, Li H Z, et al. Constitutive modeling and processing map for elevated

temperature flow behaviors of a powder metallurgy titanium aluminide alloy[J]. Journal of Materials Processing Technology, 2009, 209(12): 5363-5370.
[11] Wang K, Lu S, Fu M W, et al. Optimization of β/near-β forging process parameters of Ti-6.5 Al-3.5 Mo-1.5 Zr-0.3 Si by using processing maps[J]. Materials Characterization, 2009, 60(6): 492-498.
[12] Li M Q, Zhang W F. Effect of hydrogen on processing maps in isothermal compression of Ti–6Al–4V titanium alloy[J]. Materials Science and Engineering: A, 2009, 502(1): 32-37.
[13] Cheng Y Q, Zhang H, Chen Z H, et al. Flow stress equation of AZ31 magnesium alloy sheet during warm tensile deformation[J]. Journal of materials processing technology, 2008, 208(1): 29-34.
[14] WU Rui-heng, ZHU Hong-Tao, ZHANG Hong-bing, LIU Jian-tao, XU Zu-yao, RUAN Xue-yu. Mathematical Model for Dynamic Recrystallization of 0.95C-18W-4Cr-1V High-Speed Steel[J]. Journal of Shanghai Jiaotong University,2001,35(3):339-342.(In Chinese)
[15] Luo J, Li M, Yu W, et al. Effect of the strain on processing maps of titanium alloys in isothermal compression[J]. Materials Science and Engineering: A, 2009, 504(1): 90-98.
[16] Meng G, Li B, Li H, et al. Hot deformation and processing maps of an Al–5.7 wt.% Mg alloy with erbium[J]. Materials Science and Engineering: A, 2009, 517(1): 132-137.
[17] H. Ziegler, Progress in Solid Mechanics, (eds. IN Sneedon and R. Hill), pp.63-193, John Wiley and Sons, New York (1963)
[18] Mingjie Z, Fuguo L, Shuyun W, et al. Characterization of hot deformation behavior of a P/M nickel-base superalloy using processing map and activation energy[J]. Materials Science and Engineering: A, 2010, 527(24): 6771-6779.
[19] Y.V.R.K. Prasad, T. Seshacharyulu. Processing maps for hot working of titanium alloys[J]. Materials Science and Engineering A. 1998, 243(1-2): 82-88.